Angewandte Chemie Novit

Angewandte Novit Chemie GDCh German Chemical Society

COMMUNICATION OPEN ACCESS

Tailored Covalent Organic Framework Interphase Layer for High-Performance Anode-Free Lithium Metal Batteries

Zhaofeng Ouyang[1] | Shuang Zheng[2,3] | Shenghong Li[2,3] | Shanshan Tang[1] | Shitao Geng[1] | Shijie Li[1] | Sheza Muqaddas[1] | Qing Xu[2,3] | Gaofeng Zeng[2,3] | Hao Sun[1]

[1]Frontiers Science Center for Transformative Molecules, State Key Laboratory of Synergistic Chem-Bio Synthesis, School of Chemistry and Chemical Engineering, and Zhangjiang Institute for Advanced Study, Shanghai Jiao Tong University, Shanghai, China | [2]Advanced Separation & Conversion on Engineered Nanopore Dynamics Laboratory, Center For Low-Carbon Conversion Science and Engineering, Shanghai Advanced Research Institute (SARI), Chinese Academy of Sciences (CAS), Shanghai, China | [3]School of Chemical Engineering, University of Chinese Academy of Sciences, Beijing, China

Correspondence: Qing Xu (xuqing@sari.ac.cn) | Gaofeng Zeng (zenggf@sari.ac.cn) | Hao Sun (haosun@sjtu.edu.cn)

Received: 6 February 2026 | **Revised:** 1 June 2026 | **Accepted:** 30 June 2026

Keywords: anode-free batteries | covalent organic frameworks | interphase layer | Li metal batteries | porous materials

EDITORIAL SUMMARY

Anode-free lithium metal batteries are widely regarded as a promising route to high-energy-density storage, owing to their superior theoretical energy density, low cost, and simplified manufacturing. However, their practical application is currently limited by achievable areal capacity and rate capability. Sun, Zeng, Xu and coworkers address this challenge by introducing a tailored nitrogen-rich covalent organic framework as an interphase layer, in which abundant nitrogen sites act as lithiophilic anchors that homogenize the Li^+ flux. The obtained anode-free batteries, benefiting from the ordered framework as a stable host for uniform Li deposition, showed an impressive cycling stability at a practical areal capacity, as well as a high-rate capability, fast charging, and reliable operation under lean-electrolyte conditions. The Scientific Advisory Committee of Angewandte Chemie Novit recognizes this article as an important advance that establishes rationally designed framework materials as a versatile and programmable platform for interfacial engineering in high-performance battery chemistry.

ABSTRACT

Anode-free lithium (Li) metal batteries represent a promising candidate for high-energy-density energy storage, yet their practical implementation is hampered by the poor reversibility and kinetics of Li plating/stripping reactions, leading to limited areal capacity and rate capability. Here, we report a tailored covalent organic framework (COF) material as an efficient interphase layer for high-performance anode-free Li metal batteries. The abundant nitrogen-containing functional groups in this COF interphase layer serve as favourable adsorption sites to homogenize Li^+ flux, and its well-defined porous architecture further induces dense and uniform Li growth at high areal capacity up to 20 mAh cm^{-2}, suppressing Li dendrite growth and parasitic reactions. The resulting COF-Cu/$LiFePO_4$ anode-free batteries with a practical areal capacity of 4.1 mAh cm^{-2} exhibited decent rate capability

Zhaofeng Ouyang and Shuang Zheng contributed equally to this work.

of 3 C, indicating the potential in high-energy-density and high-rate batteries. Our results unveiled tailored COF materials as a promising platform for interfacial engineering of high-performance anode-free Li metal batteries.

1 | Introduction

The ongoing electrification of modern society demands advanced electrochemical energy storage systems with high energy densities [1–3]. Anode-free lithium (Li) metal batteries have emerged as a promising candidate featuring high energy density, low cost, and facile fabrication process [4–6]. However, their practical deployment is hampered by the limited areal capacity and rate capability, owing to the inferior reversibility and sluggish kinetics of the Li plating/stripping reactions on lithiophobic copper (Cu) current collector [7, 8]. Considerable efforts have been dedicated to addressing these challenges, including electrolyte composition [9, 10], cathode sacrificial agents [11], and anode-electrolyte interphase layers [8, 12, 13]. In particular, constructing an interphase layer on lithiophobic Cu foil represents a promising route [14]. However, the pursuit of high areal capacity above 10 mAh cm^{-2}, which is essential to enable high-energy-density anode-free batteries, remains a major challenge [4, 8].

Covalent organic framework (COF), an emerging class of crystalline porous materials, has attracted considerable attention in energy storage applications [15–19], due to the well-defined nanochannels for ion transport, robust chemical structural stability, high specific surface area, and versatile structural tunability [20–24]. These intrinsic features offer an effective platform to design new interphase materials for high-performance batteries [25–27]. For anode-free Li metal batteries, COF materials can serve as efficient building blocks for regulating Li^+ flux and accommodating Li deposition. However, it remains challenging to induce dense and reversible Li deposition based on current COF materials, particularly under an areal capacity of more than 4 mAh cm^{-2}, a benchmark required for commercial high-energy-density batteries. Therefore, tailoring COF materials for anode-free Li metal batteries are highly demanded yet challenging.

Here, we report a tailored COF interphase layer for high-performance anode-free Li metal batteries (Figure 1a). By leveraging the structural precision and functional tunability of COFs, we reveal that the abundant nitrogen-containing functional groups can serve as efficient lithiophilic sites, enhancing Li^+ adsorption and homogenizing the ion flux. More importantly, the well-defined porous architecture of the COFs serves as a stable host, guiding dense, and uniform Li deposition and effectively accommodating volume changes even at a high areal capacity of 20 mAh cm^{-2}. This synergistic effect enables the fabrication of COF-Cu/$LiFePO_4$ anode-free battery at a practical areal capacity of 4.1 mAh cm^{-2}, affording a remarkable rate capability of 3 C. Our results highlight the potential of COF materials as advanced interphase layers for anode-free Li metal batteries, and offer a viable platform for developing practical anode-free batteries.

2 | Results and Discussion

TTT-HATP-COF material was synthesized via the Schiff-base condensation of 4,4′,4″-(tris([1,2,4]triazolo)[4,3-a:4′,3′-c:4″,3″-e][1,3,5]triazine-3,7,11-triyl)tribenzaldehyde (TTT) and 4,4′,4″,4‴,4⁗,4⁗′-(triphenylene-2,3,6,7,10,11-hexayl)hexaaniline (HATP) at 120°C for 72 h (Figure 1b). The successful formation of the imine-linked framework was verified using the Fourier transform infrared (FT-IR) spectroscopy, solid-state ^{13}C nuclear magnetic resonance (NMR), and x-ray photoelectron spectroscopy (XPS). FT-IR analysis revealed the emergence of stretching vibrations at 1631 cm^{-1}, commensurate with the C═N bond the imine linkages, alongside a significantly decrease of the C═O stretch at 1701 cm^{-1}, indicating high conversion efficiency Schiff-base condensation reaction (Figure S1a). The minimal residual C═O signal is attributable to terminal groups and inherent structural defects within 2D framework. Further evidence was provided by solid-state ^{13}C NMR, which exhibited a signal at 155 ppm, assigned to both the aromatic carbons in TTT and the carbons of the C═N bonds (Figure S1b). Furthermore, the XPS analysis confirmed the presence of C═N bonds in TTT-HATP-COF, with characteristic peaks observed at 398.6 eV (Figure S1c,d). Together, these characterizations demonstrated the successful condensation reaction and the chemical structures of the TTT-HATP-COF.

The crystalline structure of TTT-HATP-COF was identified by powder x-ray diffraction (PXRD) measurement. The experimental pattern featured intense diffraction peaks at 3.32°, 5.82°, and 21.76°, which can be assigned to the (010), (110), and (001) facets, respectively, (Figure 1c). Theoretical structural models were constructed using Materials Studio 8.0 to identify the most plausible configuration. Among the evaluated stacking modes, the AA-stacking model with ***kgd*** topology showed good agreement with the experimental data, as confirmed by Pawley refinement (R_{wp} = 4.89%, R_p = 3.74%, Figure S2, and Tables S1 and S2). The refined unit cell parameters were determined to be a = 31.31 Å, b = 29.81 Å, c = 3.74 Å, $\alpha = 90°$, $\beta = 90°$, and $\gamma = 120°$. The crystallographic analysis revealed that TTT-HATP-COF possessed well-defined 2D framework with ordered 1D channels. Elemental analysis confirmed the chemical composition of TTT-HATP-COF, with C and N contents closely matching the theoretical values (Table S3).

The porosity of TTT-HATP-COF was evaluated by nitrogen adsorption–desorption isotherm measurements at 77 K. The resulting curve exhibited a combination of type I and IV isotherms (Figure 1d), with a sharp uptake at low relative pressure indicative of microporosity, and a hysteresis loop suggesting the coexistence of mesopores. The Brunauer–Emmett–Teller (BET) specific surface area was calculated to be 424 $m^2\ g^{-1}$. Pore size distribution analysis indicated that the dominant micropore at ~1.3 nm aligned well with the theoretical pore size of the ***kgd*** network, while the mesoporous signal at ~2–10 nm arose from

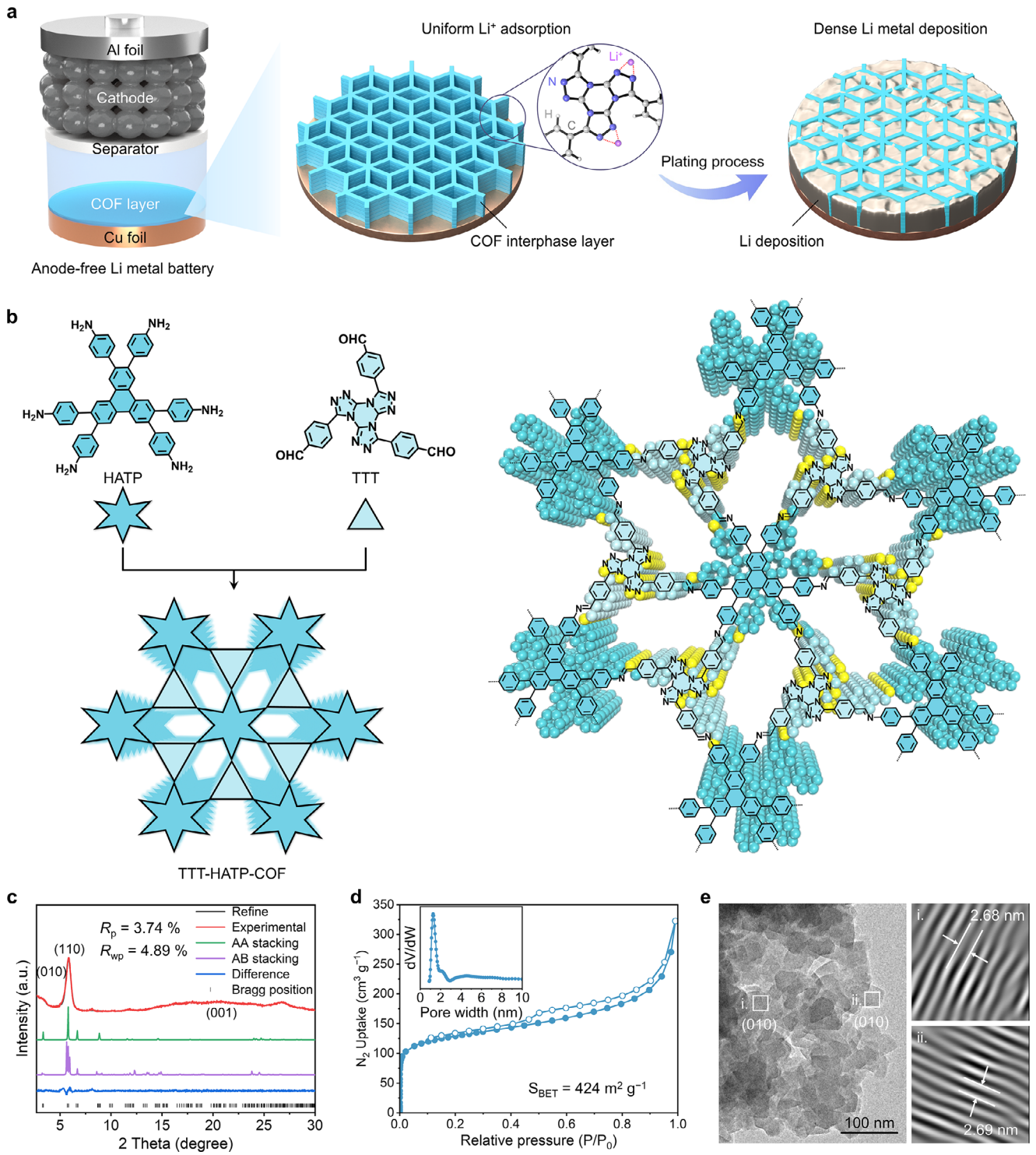

FIGURE 1 | Tailored COF interphase layer for anode-free Li metal batteries. (a) Schematic illustration of an anode-free Li metal battery using a COF-modified Cu current collector. COF interphase layer with abundant functional groups promotes the adsorption of Li ion, and acts as three-dimensional (3D) host for the improved nucleation and deposition of Li metal. (b) Schematic illustration of the synthesis process of TTT-HATP-COF. (c) Rietveld refinement of PXRD patterns of the synthesized TTT-HATP-COF. (d) Nitrogen adsorption–desorption isotherms and pore size distribution of the synthesized TTT-HATP-COF. (e) HR-TEM image and the corresponding inverse FFT images focusing on the regions marked by the white squares.

the intergranular packing voids [28, 29]. Morphological analysis by scanning electron microscopy (SEM) and high-resolution transmission electron microscopy (HR-TEM) revealed that TTT-HATP-COF consisted of submicron-sized aggregated particles (Figures S3 and S4). The well-defined lattice fringes observed in HR-TEM, assigned to the (010) crystal planes, indicating that TTT-HATP-COF possessed a high crystallinity degree (Figure 1e). Energy dispersive x-ray spectroscopy (EDS) elemental mapping further verified the homogeneous distribution of C and N elements within the COF framework (Figure S5). Thermogravi-

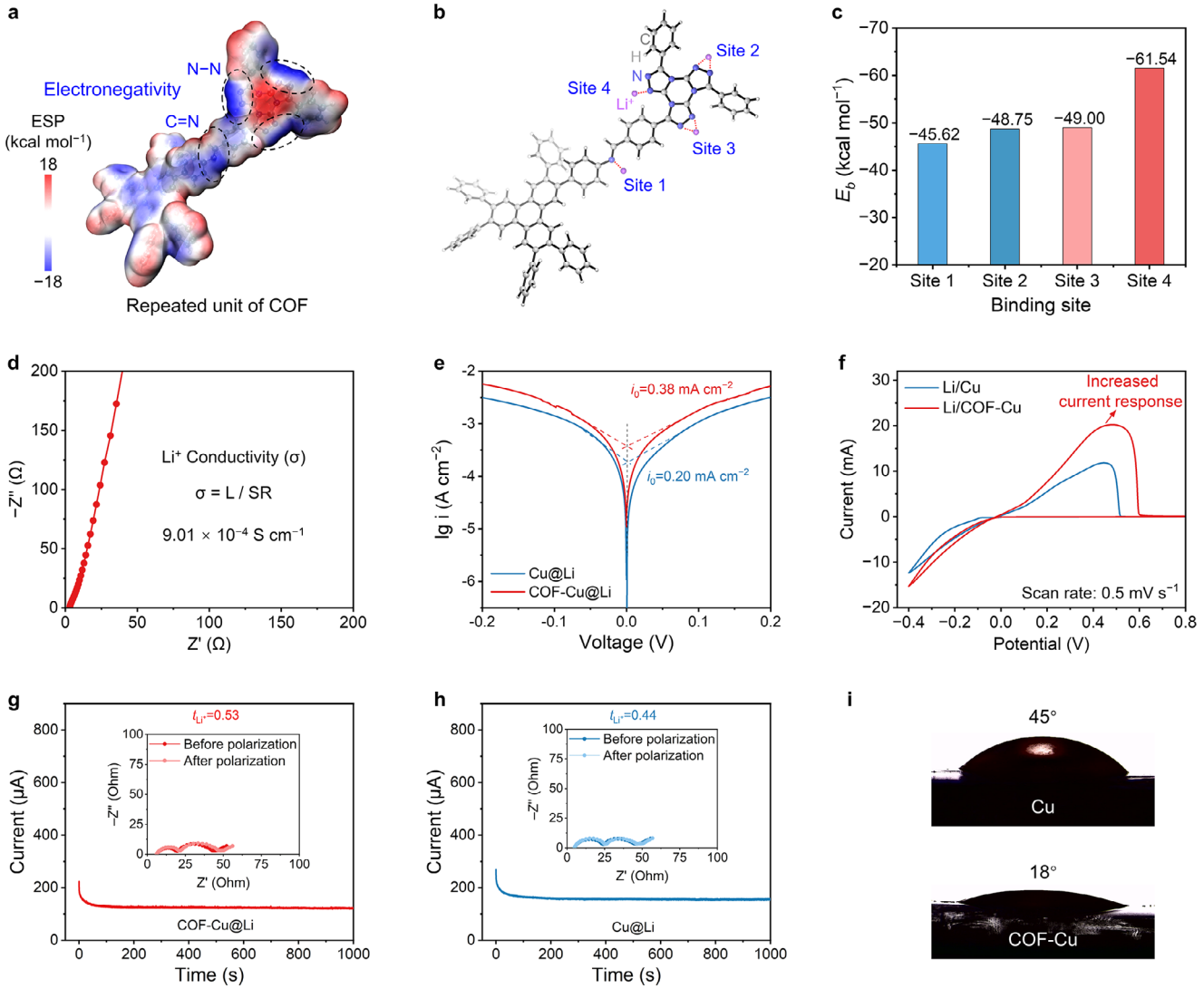

FIGURE 2 | Interaction analysis between Li^+ and COF. (a) ESP of the repeated unit of COF based on DFT calculations. (b) Geometric configurations, and (c) binding energies (E_b) of Li^+ with the four binding sites of COF based on DFT calculations. (d) Nyquist plot of symmetric cell based on COF interphase layer. (e) Tafel curves and calculated exchange current densities (i_0) of the symmetric cells based on Cu@Li and COF-Cu@Li electrodes recorded at a scan rate of 0.1 mV s^{-1} between −0.2 and 0.2 V. (f) Current–voltage curves of the Li/Cu and Li/COF-Cu cells. Chronoamperometry profiles of symmetric cells using (g) COF-Cu@Li and (h) Cu@Li electrodes, respectively. (i) Contact angles of the electrolyte on Cu and COF-Cu current collectors.

metric analysis under N_2 atmosphere revealed the high thermal stability of TTT-HATP-COF (Figure S6).

The interaction between the COF interphase layer and Li^+ was systematically investigated through a combination of theoretical and experimental approaches. Density functional theory (DFT) calculations were performed to identify the favourable Li^+ adsorption sites. The electrostatic potential (ESP) map of COF repeated unit revealed that the electron-rich nitrogen-containing functional groups served as favourable Li^+ adsorption sites (Figure 2a). Further DFT calculations on geometric configurations and corresponding binding energies (E_b) between Li^+ and four distinct binding sites within the COF indicated strong interactions, with E_b values ranging from −45.62 kcal mol^{-1} to −61.54 kcal mol^{-1} (Figure 2b,c). To validate these theoretical predictions experimentally, a COF-based interphase layer was constructed on a bare Cu foil. A slurry containing COF and lithiated Nafion (LN) (mass ratio of 2:1) in *N*-methyl-2-pyrrolidinone (NMP) was blade-coated onto the Cu current collector, yielding the COF-modified electrode (Figure S7). Laser confocal scanning microscopy (LCSM) image exhibited the high uniformity of the COF interphase layer on the Cu foil (Figure S8). Electrochemical impedance spectroscopy (EIS) profiles demonstrated that the COF interphase layer possessed a high ionic conductivity of 9.01×10^{-4} S cm^{-1} at 25°C (Figure 2d). This was consistent with the results of Tafel curves, in which the COF-modified electrode displayed a higher exchange current density (i_0) of 0.38 mA cm^{-2} compared to only 0.20 mA cm^{-2} of the Cu@Li electrode, indicating improved interfacial Li^+ kinetics (Figure 2e). This was further confirmed by the current–voltage curves, where the Li/COF-Cu cell delivered a higher current response under polarization (Figure 2f). In addition, a higher Li^+ transference number (t_{Li^+}) of 0.53 was demonstrated by the COF interphase layer, compared to only 0.44 for bare Cu, further confirming the improved interfacial Li^+ kinetics regulated by COF (Figure 2 g,h). The improved electrolyte wettability of the COF-Cu current

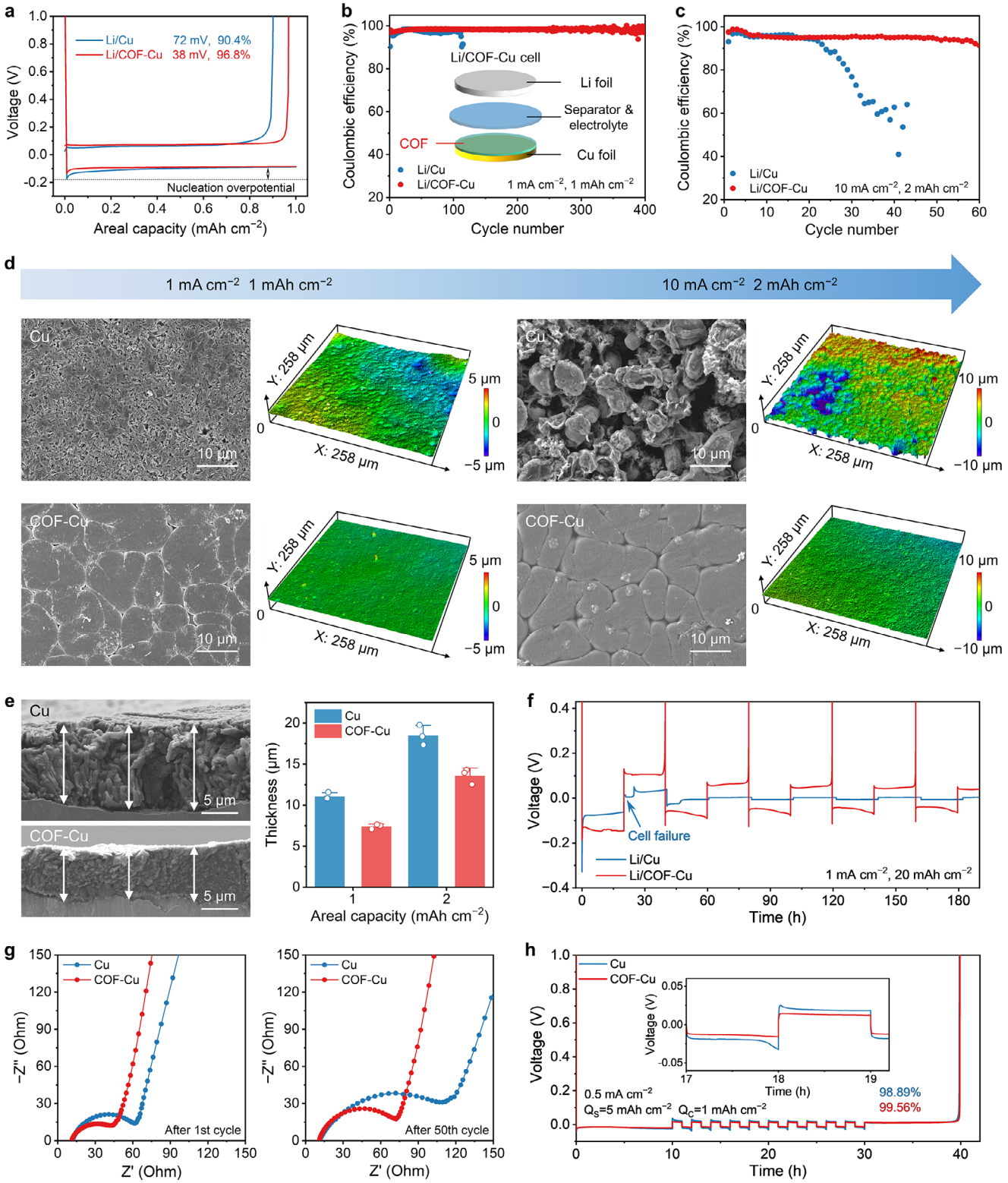

FIGURE 3 | Electrochemical properties and Li deposition morphology of Li/COF-Cu cells. (a) The initial galvanostatic charge–discharge curves of Li/Cu and Li/COF-Cu cells at 1 mA cm^{-2} and 1 mAh cm^{-2}. Coulombic efficiencies of Li/Cu and Li/COF-Cu cells at (b) 1 mA cm^{-2} and 1 mAh cm^{-2} and (c) 10 mA cm^{-2} and 2 mAh cm^{-2}. The inset shows schematic illustration of Li/COF-Cu cell. (d) SEM and 3D LCSM images of the Li deposition at 1 mA cm^{-2} and 1 mAh cm^{-2} and 10 mA cm^{-2} and 2 mAh cm^{-2} on Cu and COF-Cu, respectively. (e) Cross-sectional SEM images of Li deposition on Cu and COF-Cu at 1 mA cm^{-2} and 1 mAh cm^{-2} (left) and thickness of Li deposition on Cu and COF-Cu at 1 mA cm^{-2} and 1 mAh cm^{-2}, and 1 mA cm^{-2} and 2 mAh cm^{-2} (right). (f) Voltage-time profiles of Li/Cu and Li/COF-Cu cells at 1 mA cm^{-2} and 20 mAh cm^{-2}. (g) Nyquist plots of Li/Cu and Li/COF-Cu cells after first (left) and 50th (right) cycles, respectively. (h) Aurbach profiles of Li/Cu and Li/COF-Cu asymmetric cells. The inset showed the magnified plating and stripping curves.

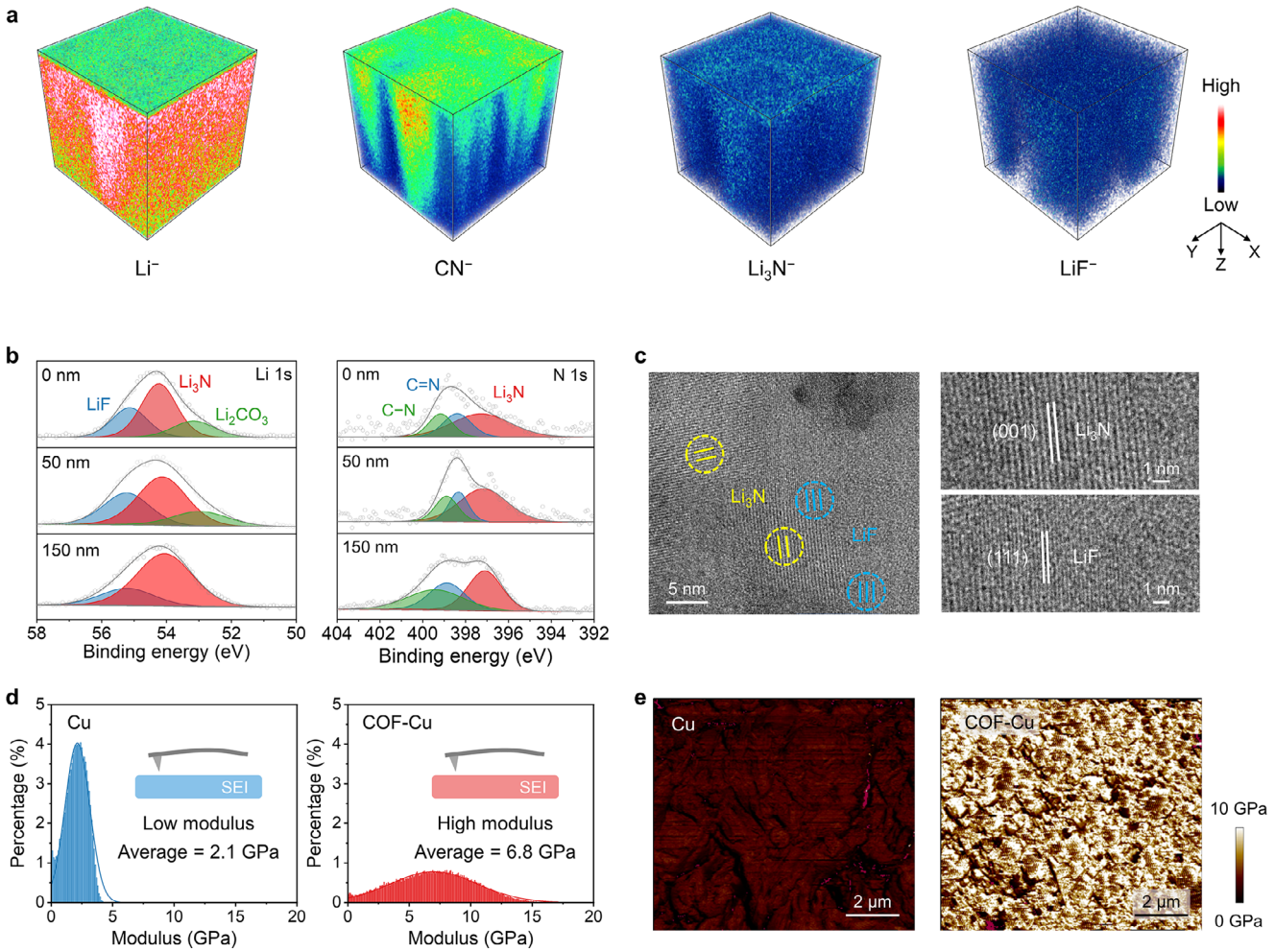

FIGURE 4 | SEI chemistry based on COF interphase layer. (a) 3D distribution of Li^-, CN^-, Li_3N^-, and LiF^- constructed based on TOF-SIMS depth scan of the Li deposition on COF-Cu after 20 cycles at 1 mA cm^{-2} and 1 mAh cm^{-2}. (b) Depth profiling of high-resolution XPS Li 1s and N 1s spectra of the Li deposition on COF-Cu surface at different sputtering depths. (c) High-resolution TEM images of the Li_3N and LiF nanocrystals. (d) DMT modulus distribution profiles, and (e) images of the SEI based on Cu and COF-Cu electrodes.

collector, as evidenced by a smaller contact angle than that of bare Cu, enabled an intimate electrode-electrolyte contact and uniform Li^+ flux at the interface (Figure 2i). These findings validated that the nitrogen-rich COF framework can serve as an ion-regulating interphase layer, facilitating Li^+ adsorption and interfacial kinetics on the lithiophobic Cu foil, thereby guiding dense and uniform Li deposition.

We evaluated the Li plating/stripping behaviours with the incorporation of the COF interphase layer in Li/Cu cells. Initial galvanostatic charge–discharge curves of the Li/COF-Cu cell displayed a significantly lower nucleation overpotential of 38 mV and a higher initial coulombic efficiency (CE) of 96.8%, compared to 72 mV and 90.4% for bare Cu, respectively, indicating promoted Li nucleation and suppressed Li loss (Figure 3a). Additionally, the COF interphase layer afforded excellent cycling stability of 400 cycles in Li/Cu cells at 1 mA cm^{-2} and 1 mAh cm^{-2}, compare to only ~100 cycles based on bare Cu (Figures 3b and S9). A similar performance advantage was maintained under a harsher condition of 10 mA cm^{-2} and 2 mAh cm^{-2}, where the Li/COF-Cu cell delivered consistent cycling stability of 60 cycles while the Li/Cu cell suffered from rapid decay after only 20 cycles (Figure 3c). The thickness of the COF interphase layer was critical to electrochemical performance (Figure S10). A sub-micrometer layer failed to effectively regulate Li^+ adsorption or suppress dendrite growth, whereas an overly thick layer of ~13.5 μm impaired cycling stability, probably by increasing interfacial resistance. SEM and 3D LCSM images further revealed the porous and mossy Li deposition morphology on bare Cu under these conditions (Figure 3d). In contrast, dense and uniform Li deposition was observed on COF-Cu, as supported by the cross-sectional SEM images (Figures 3e and S11). Even at a harsh areal capacity of 20 mAh cm^{-2}, the COF-Cu attained normal Li plating and stripping behaviours, in sharp contrast to rapid short circuit for bare Cu (Figures 3f and S12). Under a high-areal-capacity condition of 5 mAh cm^{-2}, dense and uniform Li deposition was confirmed on COF-Cu (Figure S13). The maximum current density and areal capacity achieved by the COF interphase layer are highly competitive among state-of-the-art synthetic interphase layers for Li/Cu cells (Figure S14) [30–34]. Nyquist plots of the Li/COF-Cu cell after the first and 50th cycles demonstrated a well-maintained and lower charge transfer resistance (R_{ct}), revealing suppressed parasitic reactions at the anode-electrolyte interface (Figure 3g). Aurbach profiles

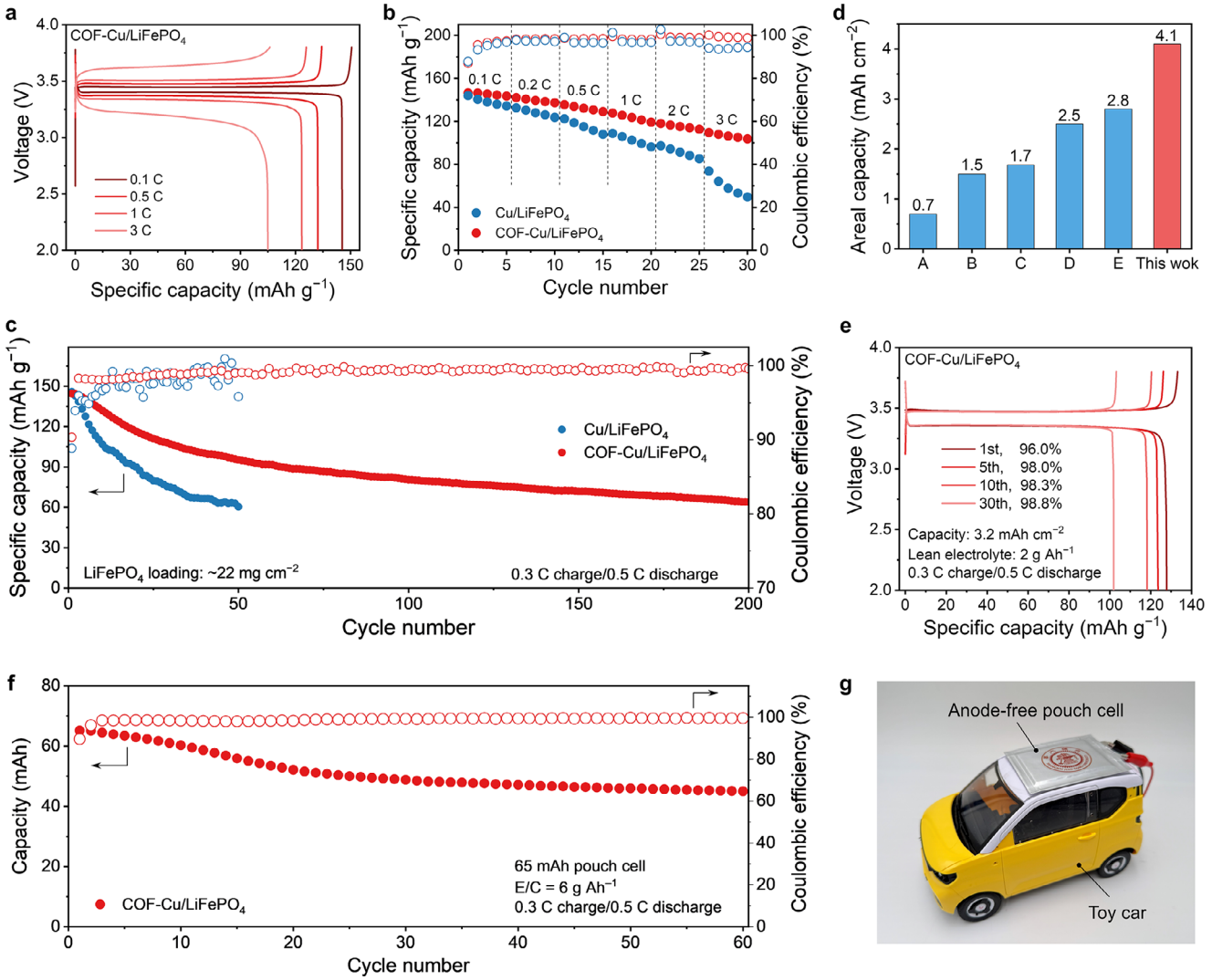

FIGURE 5 | Electrochemical performance of COF-Cu/$LiFePO_4$ anode-free batteries. (a) Galvanostatic charge–discharge curves of the COF-Cu/$LiFePO_4$ anode-free battery at increasing rates from 0.1 C to 3 C. (b) Rate performance of Cu/$LiFePO_4$ and COF-Cu/$LiFePO_4$ anode-free batteries cycling at increasing rates from 0.1 C to 3 C. (c) Cycling performance of Cu/$LiFePO_4$ and COF-Cu/$LiFePO_4$ anode-free batteries at 0.3 C charge, and 0.5 C discharge rates with the same $LiFePO_4$ mass loading of ~22 mg cm^{-2}. The batteries were first cycled for two cycles at a charge–discharge rate of 0.1 C. (d) Comparison of the areal capacity of COF-Cu/$LiFePO_4$ anode-free battery with previously reported excellent anode-free Li metal batteries based on synthetic interphase layers. A: Ref. [30]; B: Ref. [31]; C: Ref. [32]; D: Ref. [33]; E: Ref. [34]. (e) Galvanostatic charge–discharge curves of COF-Cu/$LiFePO_4$ anode-free battery under lean-electrolyte condition with an *E/C* ratio of 2 g Ah^{-1}. (f) Cycling performance of a 65 mAh COF-Cu/$LiFePO_4$ anode-free pouch cell at 0.3 C charge and 0.5 C discharge rates. (g) Photograph of a toy car powered by the COF-Cu/$LiFePO_4$ anode-free pouch cell.

further confirmed improved reversibility of the Li plating and stripping process based on COF-Cu, delivering a higher average CE of 99.56% than 98.89% of bare Cu (Figure 3h).

To unravel the mechanism for the stabilized anode-electrolyte interface, we systematically investigated the solid-electrolyte interphase (SEI) chemistry regulated by the COF interphase layer. Time-of-flight secondary ion mass spectrometry (TOF-SIMS) was employed to visualize the 3D distribution of the key components, including Li^-, CN^-, Li_3N^-, and LiF^- fragments across a COF-Cu electrode after 20 cycles (Figure 4a). Notably, the CN^- fragments, originating from the COF, exhibited a gradient distribution with higher intensity on the surface of the deposited Li metal, indicating the dual functionality of the COF layer. On the one hand, it serves as an interphase layer to suppress the parasitic reactions between the electrolyte and Li deposition. On the other hand, the underlying CN^- signals suggested that the porous COF functioned as an effective host for accommodating the volume expansion of Li deposition. Moreover, the coexistence of the pronounced Li_3N^- and CN^- signals indicated that the N-containing functional groups in COF can participate in SEI formation, resulting in the generation of Li_3N, a well-established Li^+ conductor to enhance interfacial ionic conductivity. High-resolution XPS Li 1s and N 1s spectra acquired at different sputtering depths confirmed the coexistence of Li_3N and LiF (Figure 4b). High-resolution cryogenic TEM (cryo-TEM) images further confirmed the characteristic lattice fringes of Li_3N and LiF (Figure 4c), in good agreement with the results of TOF-SIMS and XPS analysis. The mechanical robustness of SEI, a key factor in preserving interfacial integrity during cycling, was evaluated

by atomic force microscopy based Derjaguin–Muller–Toporov (DMT) modulus mapping. The COF-Cu-derived SEI showed a substantially higher modulus of 6.8 GPa, compared with 2.1 GPa for the SEI on bare Cu (Figure 4d,e). This improvement arises from the combined effect of the rigid COF interphase and the derived inorganic-rich SEI components, including Li_3N and LiF, which together suppress SEI fracture and accommodate volume changes during repeated Li plating and stripping.

The excellent interfacial stability of the COF interphase layer enables high electrochemical performance of anode-free Li metal batteries. For instance, the COF-Cu/$LiFePO_4$ anode-free battery demonstrated remarkable rate capability of up to 3 C, which maintained ~73.1% of the specific capacity at 0.1 C (Figure 5a,b), compared with only ~41.2% of bare Cu. At 0.3 C charge and 0.5 C discharge rates, the COF-Cu/$LiFePO_4$ anode-free battery with a practical $LiFePO_4$ mass loading of ~22 mg cm^{-2}, exhibited a high average CE of ~99.2% over 200 cycles, compared with only 50 cycles with a much lower average CE of ~97.6% for the Cu/$LiFePO_4$ counterpart (Figures 5c and S15). Morphology characterization further confirmed dense and uniform Li deposition on COF-Cu, in stark contrast to mossy Li deposition on bare Cu (Figure S16). Additionally, the COF-Cu/$LiFePO_4$ anode-free battery exhibited stable cycling performance even at high areal capacity of 4.1 mAh cm^{-2}, which was highly competitive among state-of-the-art anode-free Li metal batteries (Figures 5d and S17) [30–34]. Under a lean-electrolyte condition with a low electrolyte-to-capacity (*E/C*) ratio of 2 g Ah^{-1}, the COF-Cu/$LiFePO_4$ battery delivered a high-capacity retention of 79.7% after 30 cycles (Figure 5e). We fabricated a 65 mAh anode-free pouch cell based on COF-Cu, which showed decent reversibility and CEs during 60 cycles (Figure 5f), and could reliably power a toy car (Figure 5g).

Our TTT-HATP-COF features a conjugated framework with abundant nitrogen-containing groups. This molecular design enables a synergistic adsorption-conjugation effect: the delocalized π-electron system helps homogenize Li^+ distribution, while the nitrogen sites serve as lithiophilic anchors that promote Li^+ adsorption and form a Li_3N-rich SEI layer. In addition, TTT-HATP-COF possesses well-defined one-dimensional channels that provide continuous pathways for Li^+ transport. These ordered pores also serve as a nano-confining host, guiding dense and uniform Li deposition while accommodating the large volume change associated with Li plating, even at a high areal capacity of 20 mAh cm^{-2}. These chemical and structural features meet the key requirements for interphase layer materials in anode-free Li metal batteries, and provide a highly tunable platform for further improving electrochemical performance and practical viability.

3 | Conclusion

In summary, we develop a COF-based interphase layer for high-areal-capacity and high-rate anode-free Li metal batteries. The abundant nitrogen-containing functional groups serve as strong Li^+ adsorption sites to homogenize Li^+ flux. In addition, the highly ordered framework provides a stable host for inducing dense and uniform Li deposition, achieving a high areal capacity of 20 mAh cm^{-2} in Li/COF-Cu cells, due to the suppressed parasitic reactions and mitigated volume changes. This synergistic effect enables high-performance anode-free Li metal batteries at a practical areal capacity of 4.1 mAh cm^{-2}, delivering high-rate capability of 3 C, high cycling stability of 200 cycles, and stable operation under lean-electrolyte condition (*E/C* ratio of 2 g Ah^{-1}). Our findings unveil the potential of rationally tailored COF materials in anode-free Li metal batteries, opening a new avenue for high-performance anode-free batteries.

Author Contributions

Zhaofeng Ouyang: methodology, investigation, writing – original draft, writing – review and editing, validation, formal analysis, visualization. **Shuang Zheng:** methodology, investigation, writing – review and editing, writing – original draft, validation, data curation, visualization. **Shenghong Li:** methodology and formal analysis. **Shanshan Tang:** software and formal analysis. **Shitao Geng:** visualization, formal analysis. **Shijie Li:** formal analysis, methodology. **Sheza Muqaddas:** methodology, formal analysis. **Qing Xu:** project administration, supervision, writing – review and editing, conceptualization, funding acquisition. **Gaofeng Zeng:** supervision, project administration, writing – review and editing, funding acquisition, conceptualization. **Hao Sun:** conceptualization, project administration, writing – review and editing, supervision, funding acquisition, writing – original draft.

Acknowledgments

G. Zeng acknowledges the support from National Key Research and Development Program of China (2024YFE0206900). H. Sun acknowledges support from National Natural Science Foundation of China (22575145), Scientific Research Innovation Capability Support Project for Young Faculty (SRICSPYF-ZY2025049), Fundamental Research Funds for the Central Universities (25X010202131), Autonomous Project of State Key Laboratory of Synergistic Chem-Bio Synthesis (sklscbs202557), and LUI Che Woo Talent Development Fund (LCW-ZIAS-2026B05). G. Zeng and Q. Xu acknowledge support from National Natural Science Foundation of China (52303288 and 22378413), Youth Innovation Promotion Association of Chinese Academy of Sciences (E324441401), State Key Laboratory of Materials-Oriented Chemical Engineering (SKL-MCE-25B05), and Shanghai Soft x-ray Free Electron Laser Facility beamline project.

Conflicts of Interest

The authors declare no conflicts of interest.

Data Availability Statement

The data that supports the findings of this study are available in the Supporting Information of this article.

References

1. M. Armand and J. M. Tarascon, "Building Better Batteries," *Nature* 451 (2008): 652–657, https://doi.org/10.1038/451652a.

2. C. Lu, H. Jiang, X. Cheng, et al., "High-Performance Fibre Battery With Polymer Gel Electrolyte," *Nature* 629 (2024): 86–91, https://doi.org/10.1038/s41586-024-07343-x.

3. Y. Xia, P. Zhou, X. Kong, et al., "Designing an Asymmetric Ether-Like Lithium Salt to Enable Fast-Cycling High-Energy Lithium Metal Batteries," *Nature Energy* 8 (2023): 934–945, https://doi.org/10.1038/s41560-023-01282-z.

4. S. Wang, Y. Wang, Z. Ouyang, et al., "Molecular Engineering of Two-Dimensional Polyamide Interphase Layers for Anode-Free Lithium Metal Batteries," *Nature Materials* 24 (2025): 1957–1967, https://doi.org/10.1038/s41563-025-02339-y.

5. W. Chen, R. V. Salvatierra, M. Ren, J. Chen, M. G. Stanford, and J. M. Tour, "Laser-Induced Silicon Oxide for Anode-Free Lithium Metal Batteries," *Advanced Materials* 32 (2020): 2002850, https://doi.org/10.1002/adma.202002850.

6. Z. Ouyang, S. Wang, Y. Wang, et al., "An Ultralight Composite Current Collector Enabling High-Energy-Density and High-Rate Anode-Free Lithium Metal Battery," *Advanced Materials* 36 (2024): 2407648, https://doi.org/10.1002/adma.202407648.

7. J. Qian, B. D. Adams, J. Zheng, et al., "Anode-Free Rechargeable Lithium Metal Batteries," *Advanced Functional Materials* 26 (2016): 7094–7102, https://doi.org/10.1002/adfm.201602353.

8. Z. Ouyang, Y. Wang, S. Wang, et al., "Programmable DNA Interphase Layers for High-Performance Anode-Free Lithium Metal Batteries," *Advanced Materials* 36 (2024): 2401114, https://doi.org/10.1002/adma.202401114.

9. Y. Lu, Q. Cao, W. Zhang, et al., "Breaking the Molecular Symmetricity of Sulfonimide Anions for High-Performance Lithium Metal Batteries Under Extreme Cycling Conditions," *Nature Energy* 10 (2025): 191–204, https://doi.org/10.1038/s41560-024-01679-4.

10. S. Zhang, R. Li, T. Deng, et al., "Oscillatory Solvation Chemistry for a 500 Wh kg^{-1} Li-Metal Pouch Cell," *Nature Energy* 9 (2024): 1285–1296, https://doi.org/10.1038/s41560-024-01621-8.

11. T. Xu, K. Qin, C. Tian, L. Lin, W. Li, and L. Suo, "Searching for the Ideal $Li_{1+x}TMO_2$ Cathode for Anode-Free Li Metal Batteries," *Energy Storage Materials* 74 (2025): 103956, https://doi.org/10.1016/j.ensm.2024.103956.

12. L. Lin, L. Suo, Y.-S. Hu, H. Li, X. Huang, and L. Chen, "Epitaxial Induced Plating Current-Collector Lasting Lifespan of Anode-Free Lithium Metal Battery," *Advanced Energy Materials* 11 (2021): 2003709, https://doi.org/10.1002/aenm.202003709.

13. X. Song, C. Liu, A. Zhang, et al., "Interphasial Chemistry Design for Seamless Lithium Deposition in Anode-Free Lithium Metal Batteries," *Advanced Materials* 37 (2025): 2500478, https://doi.org/10.1002/adma.202500478.

14. S.-H. Kim, J.-H. Park, J. E. Lee, et al., "Conformal Deposition of Lithium Metal on Electroactive Organic Materials," *Advanced Energy Materials* 14 (2024): 2304337, https://doi.org/10.1002/aenm.202304337.

15. T. D. Bennett, F.-X. Coudert, S. L. James, and A. I. Cooper, "The Changing State of Porous Materials," *Nature Materials* 20 (2021): 1179–1187, https://doi.org/10.1038/s41563-021-00957-w.

16. Y. Jin, Y. Hu, and W. Zhang, "Tessellated Multiporous Two-Dimensional Covalent Organic Frameworks," *Nature Reviews Chemistry* 1 (2017): 0056, https://doi.org/10.1038/s41570-017-0056.

17. Y. Yang, B. Liang, J. Kreie, et al., "Elastic Films of Single-Crystal Two-Dimensional Covalent Organic Frameworks," *Nature* 630 (2024): 878–883, https://doi.org/10.1038/s41586-024-07505-x.

18. W. Qin, D. Han, X. Zhang, et al., "Redox-Active Metal-Covalent Organic Frameworks for Dendrite-Free Lithium Metal Batteries," *Advanced Materials* 37 (2025): 2418638, https://doi.org/10.1002/adma.202418638.

19. S. Zheng, S. Bi, Y. Fu, et al., "3D Crown Ether Covalent Organic Framework as Interphase Layer Toward High-Performance Lithium Metal Batteries," *Advanced Materials* 36 (2024): 2313076, https://doi.org/10.1002/adma.202313076.

20. S. Zheng, Y. Fu, C. Song, et al., "Anode-Protective Covalent Organic Framework Layer With Synergistic Cation–Anion Regulation for Dendrite-Free Lithium Metal Batteries," *Journal of the American Chemical Society* 147 (2025): 31249–31259, https://doi.org/10.1021/jacs.5c10386.

21. Y. Chen, J. He, M. Li, et al., "Regulation of Interfacial Ion Transport via Honeycomb-Architected Covalent Organic Frameworks for Lithium Metal Batteries," *Advanced Materials* 37 (2025): e12997, https://doi.org/10.1002/adma.202512997.

22. G.-X. Li, R. Kou, and A. Nguyen, "Long-Cycling Lithium-Metal Batteries via an Integrated Solid–Electrolyte Interphase Promoted by a Progressive Dual-Passivation Coating," *Nature Energy* 10 (2025): 941–950, https://doi.org/10.1038/s41560-025-01803-y.

23. C. Zhang, Z. Luo, K. Chen, et al., "Urea-Linked Covalent Organic Framework as a Li-ion Guided Channel Enabling Ultra-Stable Lithium Metal Anode in Carbonate-Based Electrolyte," *Angewandte Chemie International Edition* 64 (2025): e202500314, https://doi.org/10.1002/anie.202500314.

24. X. Wu, S. Zhang, X. Xu, et al., "Lithiophilic Covalent Organic Framework as Anode Coating for High-Performance Lithium Metal Batteries," *Angewandte Chemie International Edition* 63 (2024): e202319355, https://doi.org/10.1002/anie.202319355.

25. J. Sun, F. Kang, D. Yan, et al., "Recent Progress in Using Covalent Organic Frameworks to Stabilize Metal Anodes for Highly-Efficient Rechargeable Batteries," *Angewandte Chemie International Edition* 63 (2024): e202406511, https://doi.org/10.1002/anie.202406511.

26. Y. Kim, C. Li, J. Huang, Y. Yuan, Y. Tian, and W. Zhang, "Ionic Covalent Organic Framework Solid-State Electrolytes," *Advanced Materials* 36 (2024): 2407761, https://doi.org/10.1002/adma.202407761.

27. J. Meng, M. Yin, K. Guo, X. Zhou, and Z. Xue, "In Situ Polymerization in COF Boosts Li-ion Conduction in Solid Polymer Electrolytes for Li Metal Batteries," *Nano-Micro Letters* 17 (2025): 248, https://doi.org/10.1007/s40820-025-01768-3.

28. M. E. Carrington, N. Rampal, D. G. Madden, et al., "Sol-Gel Processing of a Covalent Organic Framework for the Generation of Hierarchically Porous Monolithic Adsorbents," *Chemistry* 8 (2022): 2961–2977, https://doi.org/10.1016/j.chempr.2022.07.013.

29. L. Li, Q. Yun, C. Zhu, et al., "Isoreticular Series of Two-Dimensional Covalent Organic Frameworks With the Kgd Topology and Controllable Micropores," *Journal of the American Chemical Society* 144 (2022): 6475–6482, https://doi.org/10.1021/jacs.2c01199.

30. O. Tamwattana, H. Park, J. Kim, et al., "High-Dielectric Polymer Coating for Uniform Lithium Deposition in Anode-Free Lithium Batteries," *ACS Energy Letters* 6 (2021): 4416–4425, https://doi.org/10.1021/acsenergylett.1c02224.

31. H. Liu, X. Yue, X. Xing, et al., "A Scalable 3D Lithium Metal Anode," *Energy Storage Materials* 16 (2019): 505–511, https://doi.org/10.1016/j.ensm.2018.09.021.

32. A. Hu, W. Chen, Y. Pan, et al., "N, F-Enriched Inorganic/Organic Composite Interphases to Stabilize Lithium Metal Anodes for Long-Life Anode-Free Cells," *Journal of Colloid and Interface Science* 648 (2023): 448–456, https://doi.org/10.1016/j.jcis.2023.06.021.

33. Y. Chen, S. Wang, T. Wang, X. Wang, H. Sun, and C. Zhu, "Preparation of Cyclic Olefin Polymers via Group Transfer Radical Cyclopolymerization for High Performance in Anode-Free Batteries," *Angewandte Chemie International Edition* 64 (2025): e202507557, https://doi.org/10.1002/anie.202507557.

34. S. Song, S. Wang, Z. Wang, H. Sun, X. Wang, and C. Zhu, "Switchable Radical Polymerization of α -Olefins via Remote Hydrogen Atom or Group Transfer for Enhanced Battery Performance," *Angewandte Chemie International Edition* 64 (2025): e202418350, https://doi.org/10.1002/anie.202418350.

35. J. Evans, C. A. Vincent, and P. G. Bruce, "Electrochemical Measurement of Transference Numbers in Polymer Electrolytes," *Polymer* 28 (1987): 2324–2328, https://doi.org/10.1016/0032-3861(87)90394-6.

Supporting Information

Additional supporting information can be found online in the Supporting Information section.

Supporting File: The authors have cited additional reference within the Supporting Information [35].